Adv. Space Res. Vol.5, No.4, pp.283-288, 1985
Printed in Great Britain.

0273-1177/85 $0.00 + .50

ON THE STRUCTURE AND DYNAMICS OF THE THERMOSPHERE

H. G. Mayr,* I. Harris,* F. Varosi,**
F. A. Herrero,* H. Volland,*** N. W. Spencer,*
A. E. Hedin,* R. E. Hartle,* H. A. Taylor, Jr,*
L. E. Wharton* and G. R. Carignan†

**NASA/Goddard Space Flight Center, Greenbelt, MD 20771, U.S.A.*
***Science Applications Research, U.S.A.*
****University of Bonn, F.R.G.*
†University of Michigan, Ann Arbor, MI 48109, U.S.A.

ABSTRACT

Thermospheric temperature, composition and wind measurements from the Dynamics Explorer satellite (DE-2) are interpreted using a three dimensional, multiconstituent spectral model. The analysis accounts for tides driven by the absorbed solar radiation as well as energy and momentum coupling involving the magnetosphere and lower atmosphere. We discuss phenomena associated with the annual tide, polar circulation, magnetic storms and substorms.

DISCUSSION

Three sources control the structure and dynamics of the Earth's thermosphere: (1) EUV radiation which is of principal importance for the global mean, the annual variations and the diurnal tides; (2) energetic particles and electric fields of solar wind-magnetospheric origin which dominate at high latitudes; (3) dynamic coupling from the lower atmosphere arising through propagating gravity waves and tides.

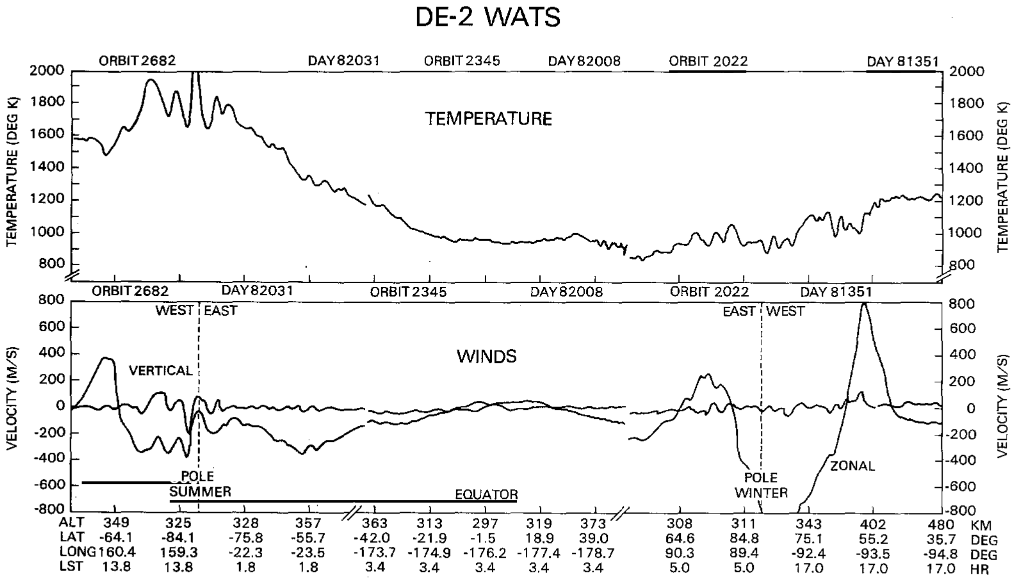

Fig. 1. Temperature and wind measurements from the WATS experiment /1,2/ on DE-2.

Data taken with the Dynamics Explorer 2 (DE-2) satellite are discussed in the light of theoretical spectral models, describing some of the important phenomena observed. Figure 1 shows pole to pole variations in the temperature and wind fields measured mainly between 300 and 400 km with the Wind and Temperature Spectrometer (WATS) on DE-2 /1,2/. It represents a composite of three data sets, matched in latitude (indicated by interruptions in the abscissa) and sampled 22 days apart on the nightside during December solstice. The largest temperatures are observed in the polar region of the summer hemisphere which is continually illuminated by solar radiation. From the equator on into the winter hemisphere the temperature does not continue to decrease but remains constant and then increases toward the winter pole, indicative of auroral energy deposition. At high latitudes, in both hemispheres, there is considerable wave activity. The data are taken under magnetically quiet conditions in winter (A_p = 6) and disturbed conditions in summer (A_p = 34) which contributes to enhance the temperature contrast between both hemispheres.

The annual variations in temperature (and composition) are driven primarily by solar differential heating. Transport and chemistry complicate the physics /3,4,5,6/. An important element is the annual tide from the lower atmosphere and the release of chemical energy from threebody recombination, which contribute to the winter anomaly in the mesospheric temperature /4,6,7/. To first order, these processes can be described in the framework of a zonally symmetric circulation. Figure 2a shows the relative temperature variations computed with a spectral model at 455 and 90 km during high levels of solar activity ($\overline{T}_\infty$ = 1400 K). The polar temperature increases from winter to summer by about 500 K, consistent with the observations. At 90 km, near the mesopause (190 K), the temperature increases by about 40 K from summer to winter. Figure 2b shows the computed relative variations in He. It reveals an increase by a factor of 10 from summer to winter poles, less than that (factor of 40) computed for low levels of solar activity. This trend is quantitatively consistent with the empirical MSIS model /8/ and can be attributed to the exospheric return flow /9/.

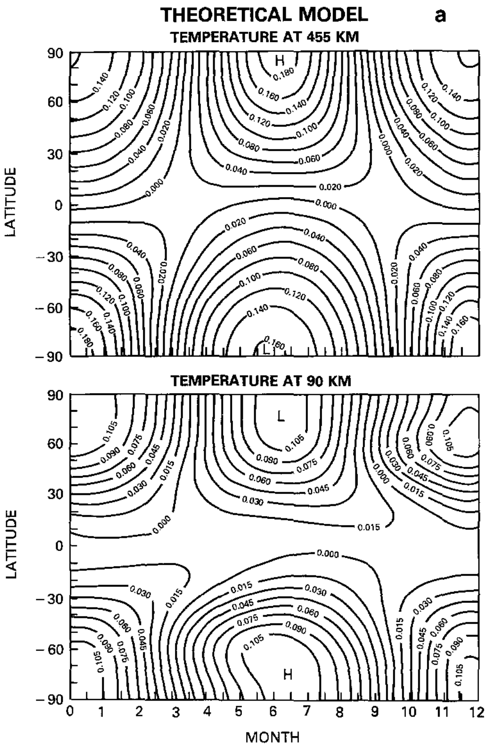

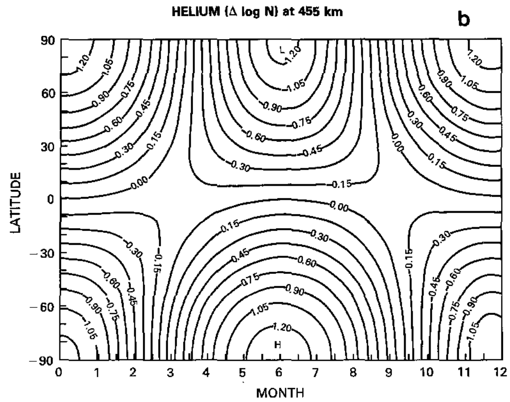

Fig. 2. Computed relative variations in the temperature (a) and He concentration (b).

In the Earth's thermosphere, the largest horizontal winds are observed at auroral latitudes. Velocities of 1000 m/sec, shown in Figure 1, are not uncommon. These winds are primarily driven by a momentum source due to ExB ion drift associated with quasi-static convection electric fields of magnetospheric origin /10,11,12/. The nature of this source is such that the resulting wind velocities are virtually divergence free and relatively inefficient in redistributing energy and mass. The wind field computed with the Volland electric field model /13/ is plotted versus (magnetic) latitude and local time (Figure 3). At 1300 LT the winds are directed primarily in the meridional direction, while at 1700 LT the zonal component is more important. This accounts in part for the large differences between the observed zonal velocities in both hemispheres (Figure 1).

On October 22, 1981, a magnetic storm occured with Ap = 72. Figure 4 shows in solid lines the density measurements from the Neutral Atmosphere Composition Spectrometer on DE-2 /14/ normalized to the quiet MSIS model /8/. We show in dashed lines data from October 18, 1981 which was quiet (Ap = 6); the differences between both data sets describe the magnetic storm effect. For comparison, we present in Figure 5 the computed storm time variations in the N_2, O and He concentrations. Associated with auroral zone Joule heating, the temperature (not shown) and N_2 concentration increase primarily at high latitudes, driving a meridional circulation which redistributes the lighter (and minor) species from high to low latitudes. The observed (and computed) O depletion at high latitudes significantly reduces the horizontal pressure gradient so that the resulting wind velocities are reduced and the temperature contrast is large (260 K increase at auroral latitudes versus 40 K at the equator).

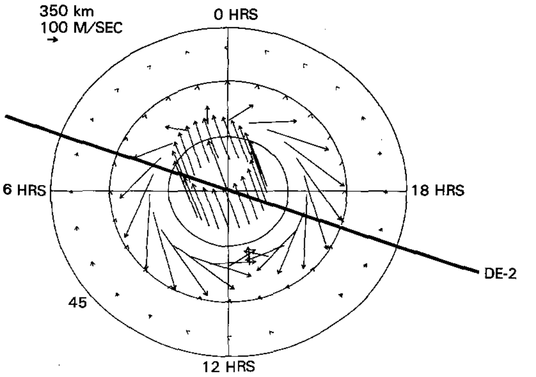

Fig. 3. Computed velocity field primarily due to E x B ion drift.

Thermospheric gravity waves are responsible for traveling ionospheric disturbances (TIDs) which are classified into large scale (wavelengths of 1000 to 4000 km) and medium scale (100 to 400 km) perturbations /15/. The large and medium scale TIDs travel with horizontal velocities of about 700 and 200 m/sec respectively. Both waves are observed at all latitudes and are correlated with magnetic activity, suggesting that the origin is in the auroral zone (Figure 1). For medium scale TIDs this represents a problem since classical gravity waves are expected to dissipate over horizontal distances comparable to their wavelengths.

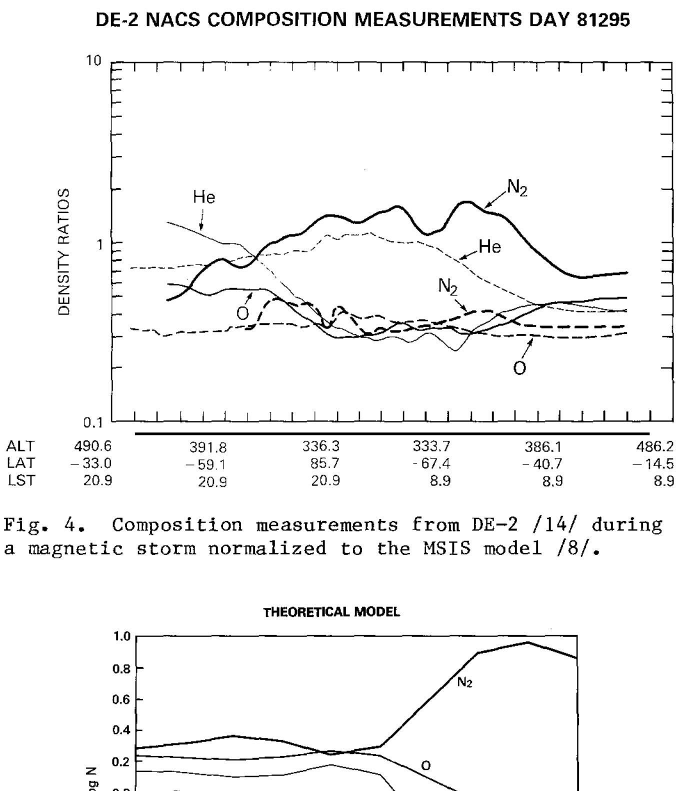

Fig. 4. Composition measurements from DE-2 /14/ during a magnetic storm normalized to the MSIS model /8/.

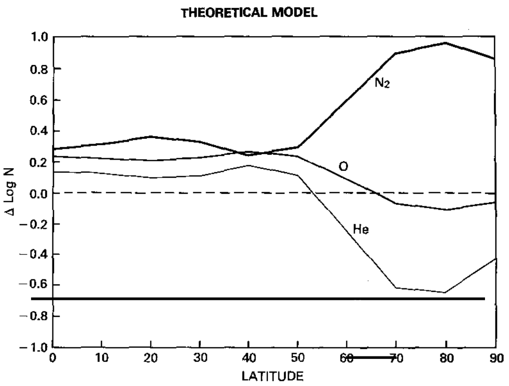

Fig. 5. Computed relative variations in composition, simulating the storm condition.

Using vector spherical harmonics, we have developed a multiconstituent spectral model to describe the short term and small scale perturbations during magnetic substorm activity. This model is discussed in the current literature /16,17/. For harmonic (0.5 hr period) Joule heating at 125 km, Figure 6a shows the computed transfer function amplitude of the temperature plotted versus altitude and horizontal wavenumber ℓ (order of Legendre polynomials). Three different wave modes are identified: (1) The quasi horizontally propagating wave which is represented by the lower cut-off and by the first, dominant resonance maximum. Its horizontal wavelength and propagation velocity (700 m/sec) are large, causing the large scale TIDs. (2) The obliquely propagating waves, generated primarily through partial reflection from the base of the thermosphere and total reflection from the Earth's surface. These waves appear as broad secondary maxima in the transfer function; their wave lengths and propagation velocities (about 400 m/sec) are much smaller than (1). They are important near the source but cannot propagate very far horizontally. (3) The ducted waves which are established in the lower atmosphere by total reflection from the Earth's surface and partial reflection from the mesopause temperature minimum near 80 km. Leaking back into the thermosphere where they origin ate, these waves have relatively short wavelengths but can travel large horizontal distances away from the source (pole to equator). The important first and second harmonic modes have propagation velocities of 250 and 170 m/sec respectively and appear in the transfer function as narrow resonance maxima. In Figure 6b the transfer function is shown at 300 km plotted against frequency ω (in cycles per day) and $c/v \propto \ell/\omega$ (where c is the speed of sound and v is the wave velocity $\omega r/\ell$; the smallest value for ω is 2). The upper limit for ω is 140 (period of about 10 minutes) and for ℓ is 200 (horizontal wavelengths of about 200 km). Figure 6b shows that individual features of the transfer function are aligned along constant values of ℓ/ω, in agreement with /18/, and, at ω = 48

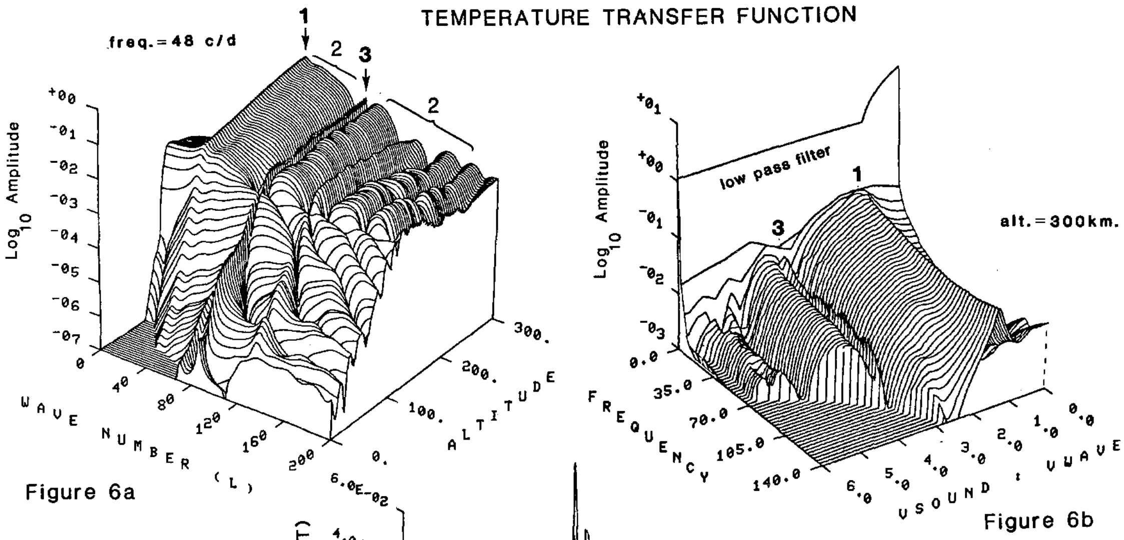

Fig. 6. Computed transfer function for the temperature, at one frequency versus altitude (a) and at 300 km versus frequency (b).

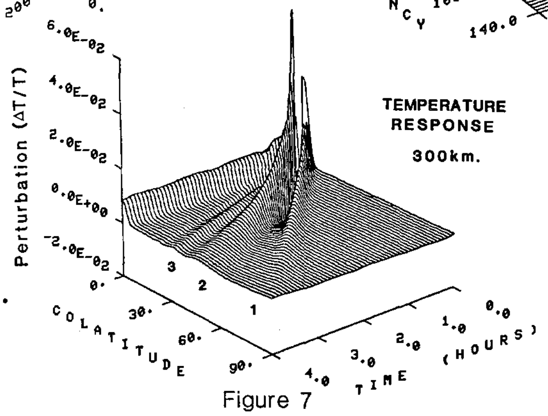

Fig. 7. Computed temperature response for a localized, impulsive heat source at the pole.

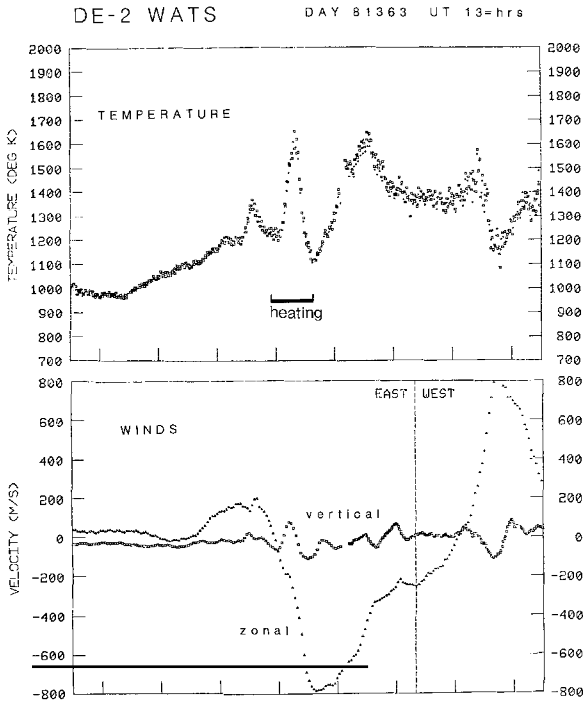

Fig. 8. Temperature and wind measurements from DE-2 during substorm on Dec. 25, 1981.

cycles per day, correspond to those discussed in Figure 6a. At low frequencies, the resonance maxima disappear, and the transfer function takes on the character of a low pass filter /19/ in which the long term (and global scale) variations are preferentially excited. To illustrate the individual wave modes, Figure 7 shows the computed temperature perturbations from a localized, impulsive heat source at the pole lasting for half an hour. We can clearly see the direct, quasi-horizontally propagating wave (labeled (1), with a speed of 700 m/sec), the reflected wave ((2), with 400 m/sec) and the ducted wave ((3), with 250 m/sec) which is weakly attenuated. In the source region, the thermospheric low pass filter is most effective, causing a slow decay in the temperature.

Figure 8 shows temperature and wind measurements /1/ from DE-2 during a magnetic substorm on December 25, 1981. The magnetic index a_p reached values of about 200 for a short period of less than three hours. Simultaneous measurements of electric /20/ and magnetic /21/ fields and precipitating particles /22/ show large disturbances confined to latitudes near 65^{o} (indicated in Figure

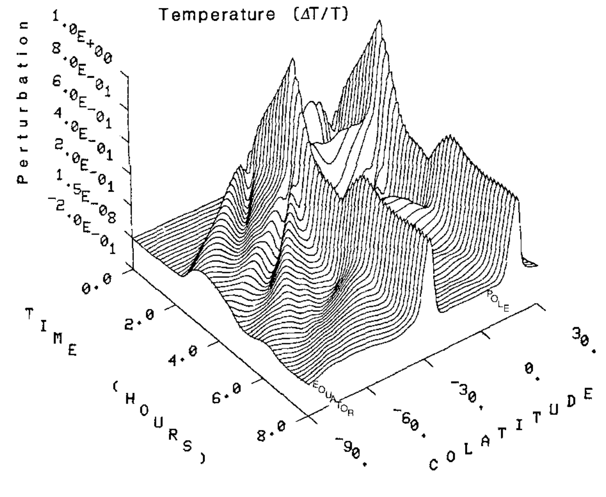

Fig. 9. Computed temperature response to a ring source versus colatitude and time.

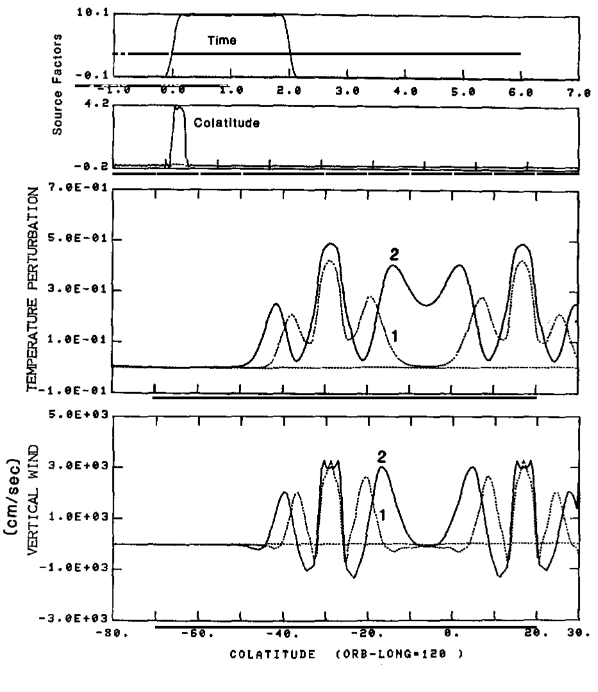

Fig. 10. Cross sections of the computed temperature and velocity perturbations 24 minutes (1) and 36 minutes (2) after the source is turned on.

8). An image of auroral emission /23/ taken from DE-1 four hours earlier indicates a ring like (oval) source geometry. On that basis, the observed perturbations are simulated with a simple model: A ring source with radius of 2500 km and 500 km wide, centered at the magnetic pole, is turned on abruptly (10 minute risetime) and after two hours is turned off again. During the transient process of energization, a broad spectrum of frequencies is prominent in the source. The frequency spectrum of the resultant disturbance is determined by the source spectrum and the transfer function. Thus the frequencies preferentially excited are those which match, through the resonances in the transfer function, the characteristic horizontal dimension of the source. This in turn produces the local ringing and the disturbances which propagate away from the source region. Figure 9 shows a three dimensional display of the computed temperature perturbation plotted versus colatitude and time. One perturbation propagates toward the equator, while a second one propagates toward the center where convergence leads to amplification. The latter wave appears to be "reflected" from the center and then propagates radially outward. These waves are launched when the source is turned on and off, producing a complicated wave pattern. About half an hour (24 (1) and 36 (2) minutes) after the source is turned on, the temperature and vertical velocity are shown in Figure 10, resembling the observations (Figure 8). For this particular simulation the excitation source was chosen to be asymmetric with respect to the equator, i.e., only one hemisphere was energized. In reality, one should expect that a similar perturbation is also launched from the other hemisphere, which can be readily described in our model. With that additional conjugate source the relative temperature perturbation near the equator would increase by a factor of two, boosting $\Delta T/T$ to almost 0.3. Perturbations of that magnitude are observed occasionally at Arequipa, Peru (near the magnetic equator) during nights with enhanced magnetic activity /24/.

REFERENCES

1. N. W. Spencer, L. E. Wharton, G. R. Carignan and J. C. Maurer, Geophys. Res. Let., 9, 953 (1982)
2. N. W. Spencer, L. E. Wharton, H. B. Niemann, A. E. Hedin, G. R. Carignan and J. C. Maurer, Space Sci. Inst., 5, 417 (1981)
3. H. G. Mayr, and H. Volland, J. Geophys. Res., 77, 6774 (1972)
4. H. G. Mayr, I. Harris and N. W. Spencer, Rev. Geophys. Space Phys., 16, 539 (1978)
5. R. E. Dickinson, E. C. Ridley and R. G. Roble, J. Geophys. Res., 86, 1499 (1981)
6. R. G. Roble and J. F. Kasting, J. Geophys. Res., 89, 1711 (1984)
7. W. W. Kellog, J. Meteorol., 18, 373 (1961)
8. A. E. Hedin, J. Geophys. Res., 88, 10170 (1983)
9. C. A. Reber and P. B. Hays, J. Geophys. Res., 78, 2977 (1973)
10. J. W. Meriwether, J. P. Heppner, J. D. Stolarik and E. M. Wescott, J. Geophys. Res., 78, 6643 (1973)

11. H. G. Mayr and I. Harris, J. Geophys., 83, 3327 (1978)
12. R. G. Roble, R. E. Dickinson and E. C. Ridley, J. Geophys. Res., 87, 1599 (1982)
13. H. Volland, Ann. Geophys., 31, 154 (1975)
14. G. R. Carignan, P. B. Block, J. C. Maurer, A. E. Hedin, C. A. Reber and N. W. Spencer, Space Sci. Inst., 5, 429 (1981)
15. T. M. Georges, J. Atm. Terr. Phys., 30, 738 (1968)
16. H. G. Mayr, I. Harris, F. Varosi, and F. A. Herrero, Part I, J. Geophys. Res., in press (1984)
17. H. G. Mayr, I. Harris, F. Varosi, and F. A. Herrero, Part II, J. Geophys. Res., in press (1984)
18. C. O. Hines, Can. J. Phys., 38, 1441 (1960)
19. H. Volland and H. G. Mayr, J. Geophys. Res., 76, 3764 (1971)
20. N. C. Maynard, E. A. Bielecki and H. B. Burdick, Space Sci. Inst., 5, 523 (1981)
21. W. H. Farthing, M. Sugiura, B. G. Ledley and L. J. Cahill, Space Sci. Inst., 5, 551 (1981)
22. J. D. Winningham, J. L. Burch, N. Eaker, V. A. Blevins and R. A. Hoffman, Space Sci. Inst., 5, 465 (1981)
23. L. A. Frank, J. D. Craven, K. L. Ackerson, M. R. English, R. H. Eather and R. L. Carovillano, Space Sci. Inst., 5, 369 (1981)
24. M. A. Biondi, and J. W. Meriwether, Jr., submitted to Geophys. Res. Let. (1984)